Marshall, *Inst. Electr. Electron. Eng. Trans.* **GE-9**, 131 (1971)]. The bands (6.8 to 7.9 μm) and (12.0 to 13.3 μm) are then "clipped off" as they contain information from atmospheric constituents and not geological (silicate) materials (*3*).
8. Both units chop the incoming radiance against an internal blackbody, set at 60°C (spectrometer) and 50° or 60°C (radiometer). The output voltages increase with lower target temperatures. Nonblackbody radiators have lower brightness temperatures (emittance at any wavelength is not equal to 1.0) at wavelengths of chemical interest (reststrahlen bands); thus, raw spectra have maxima of output voltage in these bands. Inverting the emittance data corrects this problem (*7*).
9. It is assumed that the distribution of the emittance values about their mean follows a normal distribution curve. See R. Hoffer, in *Laboratory for Agricultural Research (LARS) Bulletin 844* (Purdue Univ. Studies, West Lafayette, Indiana, 1968), chap. 3, pp. 68–71.
10. R. K. Vincent and F. J. Thomson, *Science* **175**, 986 (1972).
11. In Fig. 2, the group number is the left-hand symbol and the locality number is the right-hand number. The groups are (*B*) younger alluvium, (*C*) older alluvium, (*D*) sand over basalt, (*E*) dry lake sediments, (*F*) olivine basalt flow of spectral type 2, (*G*) olivine basalt flow of spectral type 1, (*H*) olivine basalt flow of spectral type 3. In addition, there are (*A*) rock standard granodiorite and (*I*) rock standard gabbro. The discriminant program operates in a stepwise manner to find the most powerful discriminant in *X*-dimensional space, where *X* is the number of spectral emittance values as sequentially selected by the program (*3*).
12. S. J. Garawicki is quoted [in L. F. Dellwig, *Modern Geology* (Gordon & Breach, New York, 1969), p. 63; see also pp. 72–73] as follows, "playa surface (dry lake sediments) is a hard dense compact argillic crust consisting of approximately 79% clay, 20% granular components, 0.2% accessory minerals and a trace of saline minerals."
13. J. D. Friedman [*U.S. Geol. Surv. Tech. Lett. NASA-20* (1966), p. 4] gives the composition of the basalt flows at Pisgah Crater: (flow II) total feldspar 15.4 percent and total ferromagnesian 9.4 percent; (flow III) total feldspar 38.8 percent and total ferromagnesian 5.1 percent. Flow III is more spathic than flow II, at least at the two points sampled near the crater. Herein lies one of the major problems in relating regionally variable (airborne) composition data to those of classical geological studies, which are usually from selected points.
14. See note 3 in (*7*). Standard rock I: gabbro, contains plagioclase (60 percent anorthite molecule content), augite, and a little biotite; standard rock A, granodiorite, contains biotite, quartz, epidote, and plagioclase with orthoclase.
15. The marked drop-off near 8 μm (in Fig. 2E) or the correspondingly high maxima at 8.8 μm may be due to the Christiansen effect in these fine-grained materials. This, however, does not fit for the lavas (Fig. 2, F and G).
16. The 24-channel scanner [E. M. Zaitzeff, C. L. Korb, C. L. Wilson, *Inst. Electr. Electron. Eng. Trans.* **GE-9**, 114 (1971)] has six channels selected within the thermal band, as CH 16 (6.0 to 7.0 μm), CH 17 (8.3 to 8.8 μm), CH 18 (8.8 to 9.3 μm), CH 19 (9.3 to 9.8 μm), CH 20 (10.1 to 11.0 μm), CH 21 (11.0 to 12.0 μm), and CH 22 (12.0 to 13.0 μm). The data in (*1*) would represent the combination of channels 17 to 20, ratioed with the combined channels 19 to 21. My spectral data (Fig. 2) indicate that the Pisgah geology would be more clearly defined by using channels 17, 18, and 19 (either singly or combined), ratioed to channel 20. Channel 21 would still show some effect of chemical compositions (particularly in femic rocks).
17. This research was supported in its entirety by NASA contract NAS9-7313 with NASA/MSC, Houston. This financial support is gratefully acknowledged. This is Technical Report No. 71-5, Remote Sensing Laboratory, Stanford University.

21 September 1971, revised 22 November 1971

Rock-Type Discrimination from Ratioed Infrared Scanner Images of Pisgah Crater, California

Abstract. *The radiances in two thermal infrared channels of an airborne scanner system were ratioed to produce images that recorded compositionally diagnostic emittance variations for several silicate rock types near Pisgah Crater, California.*

One of the recognized objectives of geological remote sensing has been the automatic conversion of scanner data from aircraft or satellites to geologic maps as accurate as those produced with the present techniques employed by field geologists, though on a different scale of spatial resolution. To this end, we have imaged radiance ratios of two spectral channels of data from a thermal infrared scanner that were collected during a flight over Pisgah Crater, California. We believe that these ratio images, which simultaneously record spectral and spatial information, indicate compositional differences among several types of silicate rock in the area. Data from the Pisgah Crater area, gathered by Lyon (*1*), who used an airborne infrared spectrometer, agree with ours on the spectral characteristics of the regions common to both investigations.

Silicate rocks display reststrahlen bands (departures of the spectral emittance from a value of 1.0) in the wavelength region from 8 to 12 μm, and the positions of these bands, as well as their spectral shapes, vary from silicate to silicate (*2, 3*). The only chemical parameter that has been experimentally related to the position of the reststrahlen wavelength has been SiO_2 content (*4*), though the correlation is crude. The relationship, greatly simplified, is that generally the reststrahlen positions occur at longer wavelengths for rocks containing less SiO_2.

Instead of measuring the shapes and positions of the reststrahlen bands with narrow-band spectrometers, as Lyon and Patterson (*5*) did, we monitored the reststrahlen features by ratioing the radiances detected in two medium-width ($\Delta\lambda \approx 2.5$ μm) spectral channels, in which sufficient energy is collected

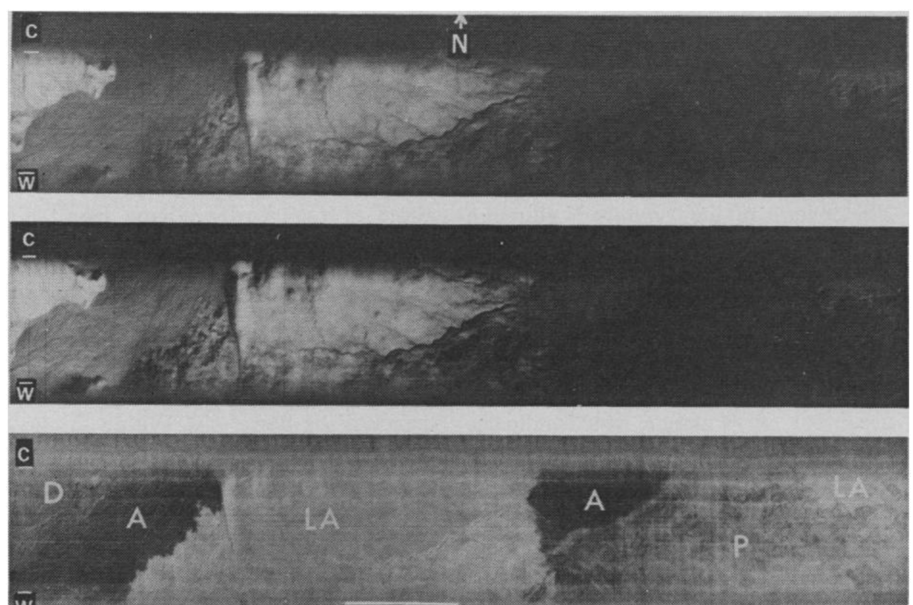

Fig. 1. Analog infrared images of the first section of a west-to-east flight line about 5 miles south of Pisgah Crater (1 mile = 1.6 km). North is toward the top. The channel 1, channel 2, and ratio R_{12} images are at the top, middle, and bottom, respectively. From left to right, the warm (bright in single-channel images) region in the westernmost part is a dacitic mountain (*D*); the adjacent colder region is alluvium (*A*), which grades eastwardly to small rock fragments and sand; and the broad, warm region is the basaltic Sunshine lava flow (*LA*). Just east of the lava flow is more alluvium (*A*), followed by playa deposits (*P*), which are mostly clay, and the southern tip of the basaltic Pisgah Crater lava flow (*LA*). The approximate edges of the cold and warm calibration plates are marked *C* and *W*, respectively. This scale is 0.5 mile per inch.

to permit imaging of either the single-channel radiances or their ratios (6). The channels are located in regions where spectral variations in the target radiance caused by differences in chemical composition are large compared to those induced by variations in target temperature. We applied a limited version of this method to data gathered over a sand quarry at Mill Creek, Oklahoma (2), which proved only that the technique could be used for the discrimination of quartz sand or sandstone from nonsilicate background targets such as carbonate rocks, vegetation, water, and man-made structures.

To test this method more rigorously, we processed scanner data gathered from a University of Michigan C-47 airplane over semiarid terrain near Pisgah Crater, California (7), an area that contains a wide variety of silicate rocks. As with the Mill Creek data, we employed a new type of two-element, trimetallic detector (mercury, cadmium, and telluride) that views each spatial-resolution element simultaneously in both spectral channels (at 3000 feet a spot 30 feet in diameter is resolved; 1 foot = 0.3 m). The approximate spectral limits of this Minneapolis-Honeywell detector are 8.2 μm to 10.9 μm (channel 1) and 9.4 μm to 12.1 μm (channel 2). The ratio of radiances in channel 1 to channel 2, which we call R_{12}, constitutes the "signal" for the ratio images. Bright and dark in the ratio images indicate high and low R_{12} values, caused by reststrahlen positions that occur at longer and shorter wavelengths, respectively. Therefore, if our analysis is correct, mafic rocks (silica-poor) should appear bright (high ratio), and felsic rocks (silica-rich) should appear dark (low ratio). This behavior is observed experimentally, as demonstrated by Figs. 1 and 2, which show analog images of two of the five lines of flight near Pisgah Crater. From top to bottom, each figure displays images of channel 1, channel 2, and R_{12} (uncorrected for temperature variations) with parts of the cool (*C*) and warm (*W*) calibration plates shown at the top and bottom, respectively, of each imaged strip (8). The straight black lines in the images of both figures are caused by noise in the image processor.

Figure 1 shows the westernmost half of a west-to-east line of flight over the Sunshine lava flows and Lavic Lake, 5 miles south of Pisgah Crater (1 mile = 1.6 km). In the ratio image, the felsic mountains and alluvium (felsic rock fragments) appear darker than the mafic Sunshine lava (basalt) and the playa material (9). The patchy appearance of the playa is primarily caused by emittance variations, because the gray level of the single-channel images is almost uniform (low thermal contrast) across the floor of Lavic Lake, of which this playa is a part. A compositional anomaly can be observed at the right-hand side of the ratio image. The basaltic Pisgah Crater lava at the top of the image and the adjacent playa material display almost the same ratio, which indicates that in these channels the spectra of the two materials may be similar, although we had expected the playa and basaltic lava to have different spectral emissivity features because of their reportedly different mineralogical composition (9). Lyon (1) has also recorded the same anomalous behavior with both airborne and ground-based spectrometers. Laboratory analyses of samples from this area are necessary before an explanation of this spectral behavior can be given.

Figure 2, a continuation of Fig. 1, shows the eastern half of the flight line across Lavic Lake. As before, in the ratio image, the boundary between playa and alluvium is sharply demarcated, and the playa material appears similar to the southern end of the Pisgah lava flow. The small, dark regions (*O*) on the northern side of the basaltic mountain (*B*) have been confirmed (on field trips) as felsic outcroppings (including dacite), which are missing from Dibblee's geologic map (10). The two most prominent dark areas (*T*) in the stream bed are regions of felsic volcanic tuff containing minor amounts of malachite, a copper carbonate. To the eye, these outcroppings of felsic tuff appear similar to the rest of the stream bed. The basaltic mountain (*B*) in the lower corner appears bright in the ratio image, which is consistent with the ratio for the basaltic mountain farther west. As in Fig. 1, felsic rocks have lower ratios (darker in the ratio image) than mafic rocks.

These images demonstrate that the ratio method is capable of enhancing emittance variations in the presence of temperature extremes that differ by no more than 25°C, with no temperature corrections. In shadowed regions (dark in the single-channel images), compositional information is still present in the ratio images. Even in its present form, the ratio method is useful for geological remote sensing over inaccessible terrain. Anyone with a thermal scanner

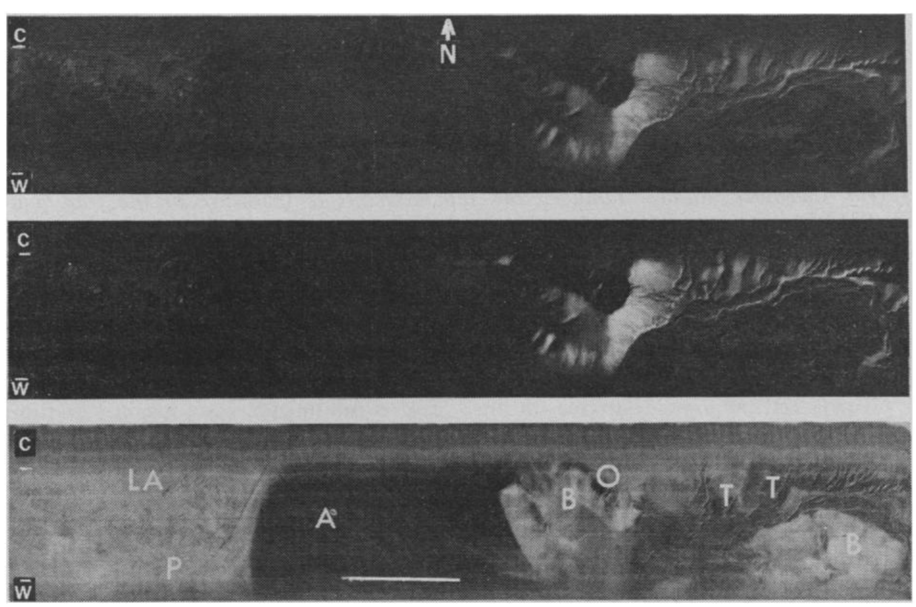

Fig. 2. Analog infrared images of the second section of a west-to-east flight line about 5 miles south of Pisgah Crater (1 mile = 1.6 km). North is toward the top. The channel 1, channel 2 and ratio R_{12} images are at the top, middle, and bottom, respectively. From left to right are Pisgah Crater basaltic lava (*LA*), playa material (*P*), alluvium (*A*), a basaltic mountain (*B*), and an intermittent stream bed (now dry), which has eroded down through the surrounding mountains of basalt (*B*). The dark regions marked (*O*) and (*T*) are felsic outcroppings (see text). The approximate edges of the cold and warm calibration plates are marked *C* and *W*, respectively. The scale is 0.5 mile per inch.

and a dual-element detector (both commercially available), or with a scanner that can accommodate two infrared-detector packages, can use this method for the discrimination of relative rock types in the two-channel mode. It is possible that the ratioing now done by an analog computer could be simulated by the simple overlaying of positive and negative transparency images; however, the compositional information in regions of lower temperature (shadows, primarily) may be lost or diminished with such a procedure.

ROBERT K. VINCENT
FREDERICK J. THOMSON
Institute of Science and Technology, University of Michigan, Ann Arbor

References and Notes

1. R. J. P. Lyon, *Science* **175**, 983 (1972); in *Proceedings of the International Symposium on Remote Sensing of the Environment, 7th* (Univ. of Michigan Press, Ann Arbor, 1971), abstr., p. 132.
2. R. K. Vincent and F. Thomson, *Proceedings of the International Symposium on Remote Sensing of the Environment, 7th* (Univ. of Michigan Press, Ann Arbor, 1971), abstr., p. 15; *J. Geophys. Res.*, in press.
3. ———, K. Watson, *J. Geophys. Res.*, in press.
4. P. A. Estep, J. J. Kovach, C. Karr, "Proceedings of the Second Lunar Science Conference," *Geochim. Cosmochim. Acta* **3**, 2146 (1971). In (*2*) we showed a crude correlation between the ratio of radiances detected at an altitude of 3000 feet by the two channels of the dual-element detector mentioned in this text and the SiO_2 content for 25 samples of silicate rock investigated by R. J. P. Lyon [*Final Report, NASA Contract NASr-49(04)* (Stanford Research Institute, Menlo Park, California, 1964), part 2].
5. R. J. P. Lyon and J. W. Patterson, *Proceedings of the International Symposium on Remote Sensing of the Environment, 6th* (Univ. of Michigan Press, Ann Arbor, 1969), abstr., p. 527.
6. F. J. Kriegler, W. A. Malila, R. F. Nalepka, and W. Richardson [*ibid.*, vol. 1, p. 97] employed radiance ratioing of adjacent channels with 12 channels in the region from 0.4 to 1.0 μm for the purpose of suppressing scan-angle and shadowing effects.
7. The flight took place on 30 October 1970 between 0800 (approximately 1 hour after sunrise) and 0840 hours, Pacific time, at an above ground altitude of 3000 feet. It was a clear morning, with relative humidity below 25 percent and a ground-level air temperature of approximately 5°C.
8. The maximum temperature difference detected between the hottest and coldest targets on the ground was approximately 25°C.
9. P. F. Kerr and A. M. Langer, in *Environmental Research Papers No. 96*, J. T. Neal, Ed. (U.S. Air Force Cambridge Research Laboratory, Bedford, Massachusetts, 1965), p. 31. They describe the playa material as 79 percent clay, 21 percent granular components (predominantly quartz and feldspar), 0.2 percent accessory minerals, and a trace of saline minerals (halite, carbonate, and sylvite).
10. T. W. Dibblee, Jr., *Miscellaneous Geological Investigations Map I-472* (U.S. Geological Survey, Washington, D.C., 1966).
11. Supported by NASA contract NAS 9-9784. We thank Dr. William Fischer, U.S. Department of the Interior, and Dr. Archibald Park, National Aeronautics and Space Administration headquarters, for their prompt decision-making on this flight, which saved a year of waiting for these results. We also thank the University of Michigan flight crew for their excellent data collection.

21 September 1971; revised 1 December 1971

Peripheral Thermoregulation: Foot Temperature in Two Arctic Canines

Abstract. *Arctic foxes and gray wolves maintain their foot temperature just above the tissue freezing point (about −1°C) when standing on extremely cold snow, or when the foot is immersed in a −35°C bath in the laboratory. Proportional thermoregulation stabilized the subcutaneous temperature of the foot pad to a precision of ± 0.7°C (largest deviations). Selective shunting of blood-borne body heat through a cutaneous vascular plexus in the foot pad accounted for more than 99 percent of measured heat loss from the pad surface. Maximum energetic efficiency is achieved because the unit of heat exchange is located in the pad surface which contacts the cold substrate rather than throughout the pad.*

Terrestrial mammals survive in the arctic because of morphological and physiological adaptations to cold (*1*). Thick, closely spaced fur, for example, protects the trunk from excessive heat loss, although the legs which are relatively more exposed due to thin fur and high surface area to mass ratio may be predominantly protected by physiological mechanisms (*2*).

Previously attention had focused on countercurrent heat exchange in the legs wherein heat of the descending arterial blood is cooled as it warms returning venous blood. Heat flow to the feet is minimized, resulting in low foot temperature and lower heat loss to cold surfaces (*3*). How the foot temperature is maintained near 0°C even when animals are standing on substrates 50°C or more colder has not been accounted for. This study demonstrates that in the arctic fox and gray wolf the mechanism of this important physiological adaptation is increased blood flow to the foot pad surface during exposure to cold.

A colony of adult arctic foxes (*Alopex lagopus*) and gray wolves (*Canis lupus*) at the Naval Arctic Research Laboratory, Barrow, Alaska, was maintained year around in welded steel enclosures exposed to prevailing weather, typically 5°C in summer and −30°C in winter. During experiments the animals were lightly anesthetized with α-chloralose (50 mg/kg, intraperitoneal) which rendered them unconscious but capable of myoclonic responses to loud sounds. Vascular and thermoregulatory autonomic reflexes appeared to be intact, and normothermia was maintained (*4*). A net hammock suspended the animals in the laboratory in a normal standing posture. One hind foot was submerged to the ankle in a well-stirred mixture of ethanol, ethylene glycol, and water (1 : 1 : 1) cooled to −38°C with Dry Ice while temperatures of the foot were recorded continuously during immersion for up to 7½ hours.

A disk surface thermistor (*5*) taped under a hemisphere of polystyrene foam (10 mm in diameter) measured skin surface temperature. Because of incomplete insulation from the cold bath, temperature occasionally registered several degrees too low in this thermistor, but the instrument accurately followed shifts in skin temperature with a resolution of 0.05°C. Three 0.25-mm-diameter thermistor beads (*6*), embedded in a Teflon capillary tube (1.2 mm outside diameter) and inserted into the center of the foot through a 15-gauge needle from the ventral pad surface, sensed temperatures about 2 mm, 8 mm, and 12 mm inside the pad skin surface. Rectal, contralateral foot pad surface, bath, and room air temperatures were simultaneously monitored with an accuracy of ± 0.1°C. Rate of heat flux from the foot pad to the bath was measured with a heat flow transducer (*7*) taped against the pad. Thirty-nine experiments were conducted on 3 adult foxes and on 21 wolves varying in age from 3 weeks to 7 years.

In both species immersion of the foot in the cold bath caused an immediate drop in foot temperature (Fig. 1), albeit not to, or below, the tissue freezing point (*8*). One of two response patterns ensued: (i) either the pad surface temperature plateaued at a mean 12.8° ± 1.4°C ($\bar{X}$ ± standard error) for a period of about 45 minutes and then dropped to 1.5° ± 0.9°C for an indefinite period; or (ii) the pad temperature initially fell to 3.9° ± 0.9°C and then remained constant throughout the immersion. In 1-year-old wolves the first response with its apparent poor